Final Report

AMPC
AUSTRALIAN MEAT PROCESSOR CORPORATION

Remote Operations - Shadow Robots

Remote Operations - Shadow Robots - Stage 1

Project Code
2021-1224

Prepared by
Prof Peng Shi and Dr Xin Yuan

Date Submitted
30/06/2022

Published by
AMPC

Date Published
30/06/2022

Contents

1.0 Executive Summary

This project will provide a concept design of remote-controlled shadow robots in the meat processing industry, in which the robotic arms can be controlled remotely and duplicate human motions in real-time. The project aims to eliminate direct human involvement in high-risk operations and retain human workforces under safer and better working conditions. At this stage, the project has successfully developed a conceptual shadow robot system, in which the operator wears a 3D printed exoskeleton device with potentiometers attached to measure her/his joint angles and drives two UR5 robotic arms to achieve the human poses. To demonstrate the system's capability and functionality, the testing operator drives the robotic arms to pick up an object, hand it over to the other arm and drop it off at a desired reachable position. This proof of concept development demonstrated that the designed shadow robot system could be used to duplicate human motions. This report introduces the system design of the shadow robot and the methods of detecting human poses and transforming them into robot motions. The report also discusses some issues that need further investigation, which will potentially improve the system's performance and functionality.

2.0 Introduction

We conducted literature reviews in the project-related fields, including network control systems, human-machine collaboration, and robotic systems. The following background knowledge is related to the project-designed shadow robot system.

Network control systems

A networked control system (NCS) is a class of control systems wherein the control loops are closed through a communication network. Compared with conventional control systems where wires connect all the components, NCSs have many advantages, such as low installation and maintenance costs, easy reconfigurability, and high reliability and flexibility. This project will develop an NCS that takes input signals from controlling devices and sends control signals to operate the robotic arm platforms. Key constraints and challenges include network-induced delay, packet disorders and dropouts, cyber-attacks and limited network resources, which encouraged us to focus more on the design and implementation of NCSs, especially under cyber-attacks.

Human-machine collaboration

Morden advanced manufacturing technologies establish hyper-connected industrial ecosystems that are not limited to automated production lines but also facilitate multi-task and multi-platform integration, which, in particular, fosters the creativities and cognitions of human-machine collaboration. To accommodate that, manufacturers are emerging in the digital transformation of industries to build an environment where humans can work collaboratively with robotic and autonomous systems. Aside from the productivity of machines and the intelligence of humans, human-machine collaboration is deemed a more practical approach by future manufacturers. The shadow robot is a typical example of human-machine collaboration, wherein the human operates the devices directly based on visualisation and sensor feedback, and the robot mimics human motions and performs tasks as the human.

Robotic systems

Robotic systems are commonly used by manufacturers to automate manufacturing processes which can reduce labour and production costs, production time and human risks. While industrial robots are still dominating the manufacturing industry, some operations still require manual labour and can not be fully automated in a conventional way. Particularly, in the meat processing industry, processes are highly dynamic.

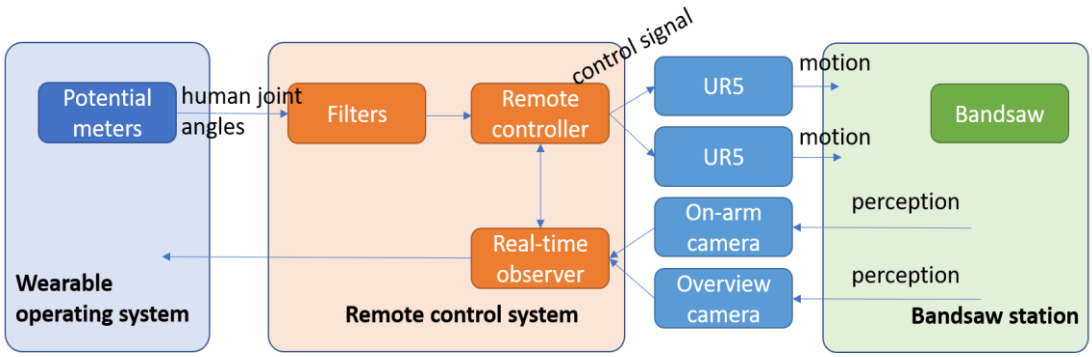

Figure 4.1 The shadow robot system structure

3.0 Project Objectives

To evaluate the concept of shadow robot enabled solutions and ascertain:

1. Where the solution can be deployed now within the industry

2. Where the solution could be deployed now, with minor changes (for example, additional vision and sensing required)

3. Where the solution could be evolved for future deployment.

4.0 Methodology

We designed the high-level structure of the shadow robot system and assembled the physical robotic arms onto a dual-arm base.

4.1 System structure design

Figure 4.1 shows the system structure of this remote-operating shadow robot. There are two main sub-systems which are the wearable operating system and the remote-control system. The operating system includes sensors and potentiometers, which will be attached to an operating suite and worn by the human operator, and human motion data

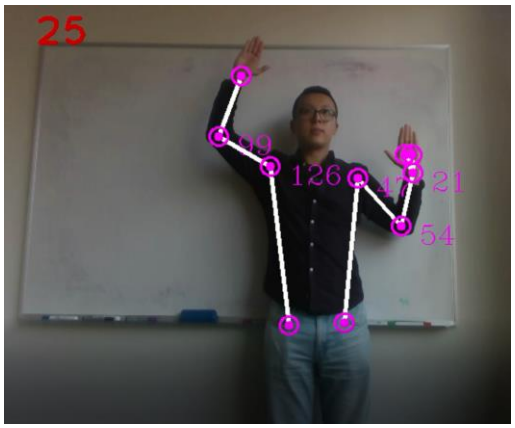

Figure 4.2.1.1 Vision-based motion

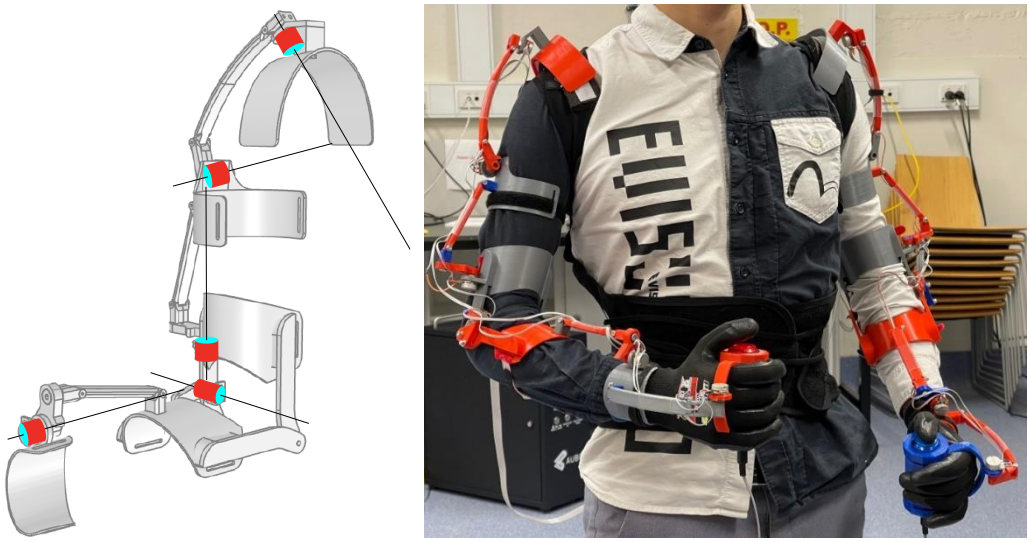

Figure 4.2.1.2 The wearable exoskeleton

are outputted to the remote-control system, which analyses the input data and converts them into control signal which drives the physical platforms (UR5 robotic arms) to work on a bandsaw station. An overview camera is set on top of the bandsaw station, and on-arm cameras are attached to the robotic arms. Visual images are fed to a real-time observer, which allows the human operator to monitor the situations.

4.2.1 Human motion sensing and detection

Based on our design, robotic arms are controlled directly by human motions. Therefore, it is essential to develop effective methods to detect human motions. We attempted and developed two approaches: vision-based pose detection and joint angle sensing with potentiometers.

Vision-based motion detection

The initial approach we tested is to use a camera to capture real-time images of the operator, and the images are processed by OpenCV Human Pose Estimation algorithm. An example of detection is illustrated in Figure 4.2.1.1. It can detect human poses in real-time and calculate each joint angle and human pose kinematic. This method has a significant advantage in its setup, which does not need to take any training for the human operators to get familiar with using the equipment. However, processing in real-time with a high refreshing rate requires enormous computational power, yet the light conditions of the operating zone are also essential to collect clear images for recognition. Another potential issue is that not wearing any devices does not provide any direct feedback (senses of resistance force) to human operators. It will be difficult for the operators to control robotic arms precisely.

Wearable exoskeleton device

Another approach for sensing joint angles is to use a wearable exoskeleton assembled by 3D printed brackets with potentiometers attached to the joints. Figure 4.2.1.2 shows the design of the exoskeleton. The graph on the left indicates the structure and mechanism that can be attached to the arms of the human operators, and each bracket can be tightened by adjustable velcro tapes. The red cylinders indicate potentiometers attached for measuring joint angles.

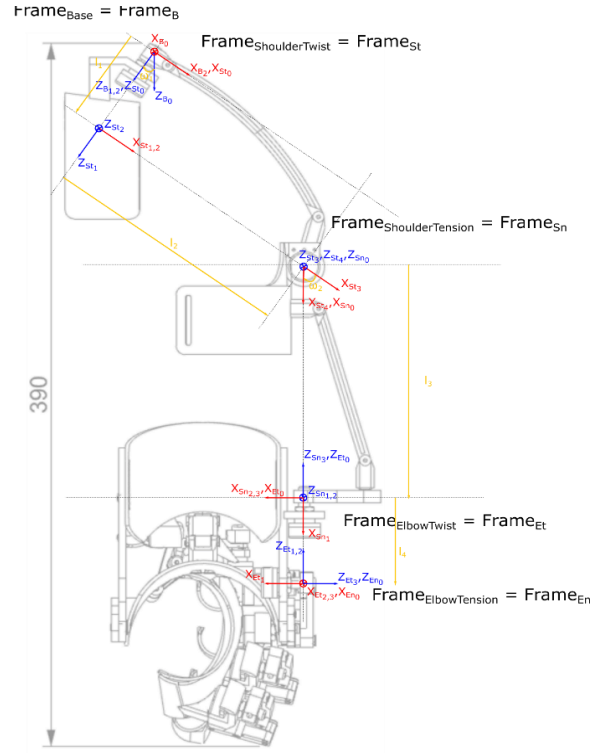

Figure 4.2.1.3 The wearable exoskeleton

Real-time values of all potentiometers are read by a microprocessor (Arduino MKR1000) through analog inputs and transmitted to the host computer via serial communication. The raw analog signals have noise, and it will potentially provide inaccurate inputs for controlling the robotic arm joints and cause vibrations on the physical platforms. In order to cancel the noise, low-pass filters are implemented to smooth out analog inputs from each potentiometer. While the wrist responds faster than the shoulder, the cut-off gain of low joints is higher for the low-pass filter.

The wearable exoskeleton joints have six frames for the shoulder, elbow and wrist: Shoulder Twist, Shoulder Tension, Elbow Twist, Elbow Tension, Wrist Twist and Wrist Tension. Figure 4.2.1.3 indicates the detail for coordinates defined for all frames. The details of calculated transfer matrixes between each frame are attached to appendix 1.

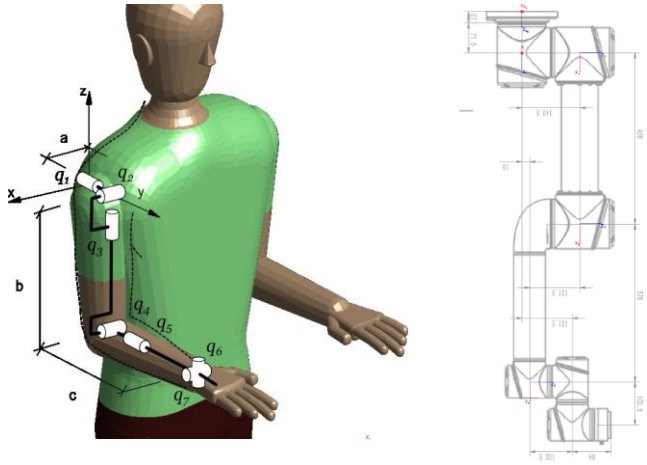

Figure 4.2.2 Convert human poses to robotic arm motions

4.2.2 Remote-control system

The remote-control system provides an interface between joint angles detected by potentiometers and UR5 robotic arms. It converts the human pose to robotic arm motions (Figure 4.2.2). The remote-control system has two main modules: the communication interface and the arm controller. The remote-control system also receives a real-time camera feed from the on-arm camera and the overview camera, and the real-time images from these cameras are displayed on a screen to provide more information for the human operator to observe the situation.

Communication interface

The microprocessor collects real-time data from all potentiometers and communicates with the host computer via serial communication. All values of potentiometers are converted to joint angles, packed in a string data package, and transmitted with a frequency of 200 Hz. Once the host computer receives the data, they are decoded and transformed into each joint's robotic arm frames. Then, these robotic arm joint angles are set to be the target angles for the arms controllers. The target angles are updated in real-time.

Arm controller

After the host computer calculates the target joint angles, it will request all current joint angles from the robotic arm, as feedback, to calculate the control values and output to each joint. We are using a PID controller for each robotic arm joint, $u(t) = K_p e(t) + K_i \int_0^t e(t)dt + K_d \frac{de(t)}{dt}$, where $e(t) = target\ joint\ angle - current\ joint\ angle$, and K_p, K_i, and K_d are the proportional, integral and derivative gains, respectively. Then, the control value will send through to the robotic arm as a packet via an Ethernet connection.

4.2.3 Bandsaw station

The physical robotic arms are attached and operate on a bandsaw station, a piece of the standard equipment used by all beef processors. An overview camera is attached on the top to monitor the blade and cutting points. This design provides high feasibilities for processors to deploy this innovative system with only minor changes.

5.0 Project Outcomes

We have developed and tested the shadow robot system in a virtual simulation environment and with the physical robotic arms to test feasible approaches. With the virtual simulation, we tested the vision-based motion detection and potentiometer-based sensing, and we concluded that the vision-based approach is not suitable for this project due to its limitation in detecting three-dimensional poses.

5.1 Virtual environment testing

We conducted single-arm virtual simulation tests in the CoppeliaSim 3D virtual environment. A pre-assembled 3D model of UR5 robotic arm is imported to the virtual environment. It simulates all physical aspects, measurements and constraints of a physical robotic arm, including forward and invert kinematics and all joint motion response. We programmed a basic control algorithm in an associated child script of the 3D robotic arm, which can drive each joint on the virtual arm according to the inputted desire angles. The virtual simulation provides a safe and reliable testing environment for the proof of the design. It also allows access to all operation data for analysing motion detection performance and the communication module.

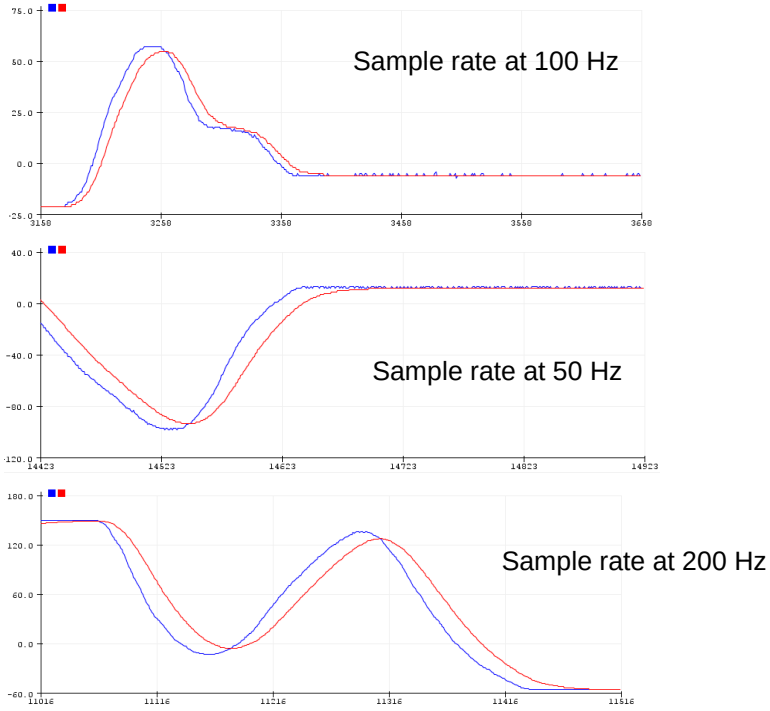

Figure 5.3.1 Low-pass filter testing

Using the virtual 3D robotic arm, we tested the vision-based motion detection. We also built up the communication module as an interface to communicate with an Arduino microprocessor via serial communication and used it to test the wearable device with potentiometers for joint angle sensing.

5.2 Vision-based motion detection testing

As the vision-based approach introduced in section 4.2.1, we developed a motion detection module using the OpenCV Human Pose Estimation algorithm. Vision inputs are fed into and processed on the host computer. The host computer detects the body parts and poses and tracks the motions of the operator. With a frame rate of over ten frames per second, the host computer can provide real-time detection and calculate each joint angle of the operator's arms. The joint angles are inputted to the running script of the virtual robotic arm and drive it to achieve different poses. However, due to the limitation of the visibility of the camera, only the detections on the x-y frame (perpendicular to the camera view direction) are valid and precise. The virtual robotic arm can only achieve two-dimensional poses. In order to

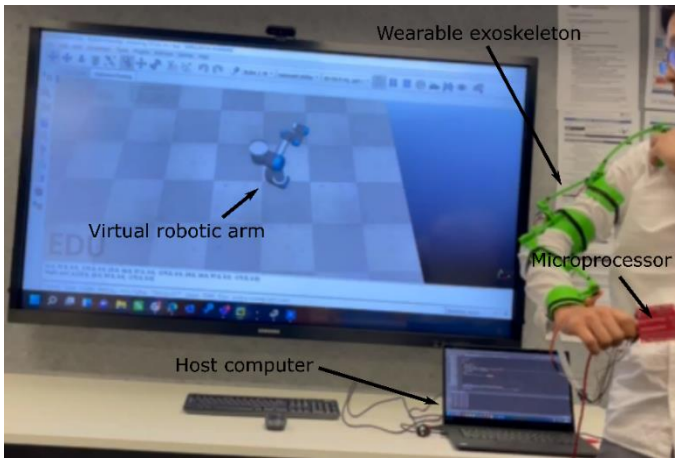

Figure 5.3.2 Virtual arm testing with

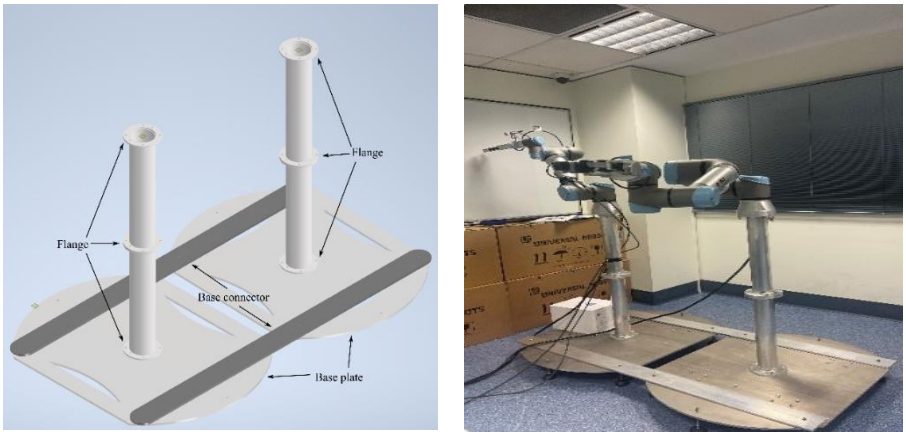

Figure 5.4.1 Dual-arm

improve the detection of effective three-dimensional poses, additional cameras will need to be installed to observe the poses and motions of the operator from both sides. It will require more extensive computational power to fit the requirements of real-time detections. Therefore, vision-based motion detection is not feasible.

5.3 Wearable exoskeleton testing

Based on the evaluation of the vision-based motion detection, we decided to use the wearable exoskeleton with potentiometers to detect angles of the joints (introduced in section 4.2.1). We 3D printed all brackets of the exoskeleton and attached potentiometers to measure all six joint frames, and an addition button is attached to trigger the open/close of the gripper. We coded the microprocessor to read analog inputs and converted them into joint angles. Discrete low-pass filters are coded on the microprocessor to smooth out the input signals. Figure 5.3.1 shows the comparison results between raw and filtered signals. The blue line indicates the raw analog input data from the potentiometer, and the red line indicates the filter output. Based on different frequencies, the effectiveness of the low-pass filter changes.

Figure 5.3.2 shows the setup of the virtual arm and physical exoskeleton testing. The filtered human joint angles are inputted to the host computer and converted into robotic arm joint angles, which are inputted to the CoppeliaSim 3D virtual environment with the 3D UR5 robotic arm. It can drive the robotic arm to achieve the desired joint angles and

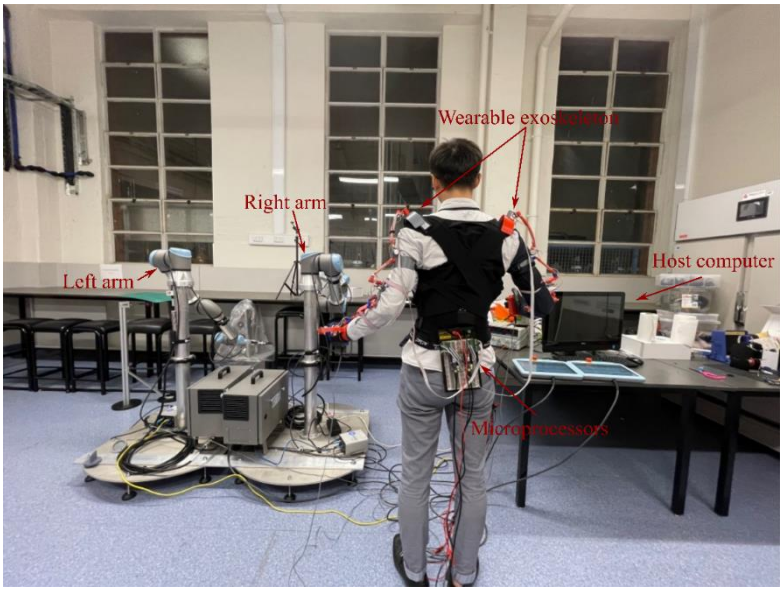

Figure 5.4.2.1 Physical test setup

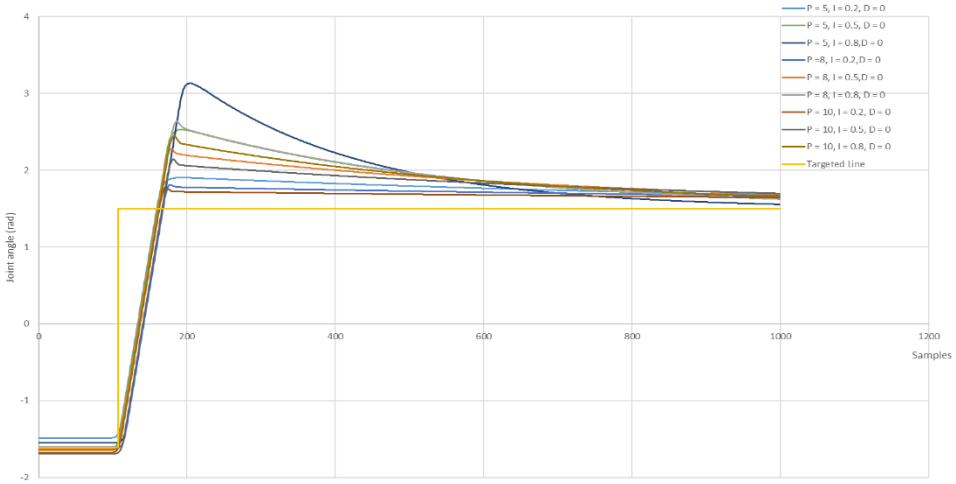

Figure 5.4.2.2 Tuning controller

duplicate human poses. The outcome demonstrated that the transfer matrixes and a wearable exoskeleton with potentiometers were developed successfully. However, calibrations are required for the physical platform testing.

5.4 Physical testing

5.4.1 Dual-arm base

In order to fit the design of operating two UR5 robotic arms, UoA designed a dual-arm base. Figure 5.4.1 shows the design and assembled dual-arm base.

The dual-arm robotic arm based is built by connecting two individual arm bases. The connectors are used to fix up the relative distance between two arms. Each base has two 500mm metal pipes with flanges. This design will allow the height of the arm to be adjustable and reconfigurable. The arms can be lower or higher based on the required setting in the later stage. The flange is designed based on the drilling of UR5 bases. It can be redesigned if different robotic arms are used. Four omni-direction castors are installed under each base plate for easy transportation, and adjustable levelling feet are installed for holding up the positions while robotic arms are at the operating station.

5.4.2 Physical robotic arm testing

We processed to test the wearable exoskeleton with the physical robotic arm platforms. Figure 5.4.2.1 shows the physical testing setup. The operator wears both sides of the exoskeletons, and all potentiometers are connected to the analog input pins of microprocessors (MKR1000) and powered externally from a DC voltage supply of 3.3V. Like the virtual environment testing, the microprocessors communicate with the host computer via serial ports to send through filtered joint angles. The host computer then calculates the desired robotic arm angles and determines the control speed of each joint based on the feedback of the current joint angles. The control signals are sent to the robotic arms via network communication.

Based on our testing and evaluation, we find the best control gains at $K_p = 10$, $K_i = 0.2$, and $K_d = 0$, which provides a fast responding time and reliable saturation speed. Figure 5.4.2.2 shows the experimental results of testing different control gains.

We have successfully implemented and tested the designed shadow robot system. Some testing video is available in a BOX cloud drive, and the link is provided in appendix 2.

6.0 Discussion

During this development, we found that several issues can be resolved to improve the system's performance.

Gripper control

Currently, we attached a OnRobot RG6 two-finger gripper on each robotic arm. This device does not provide a flexible gripping mechanism, and it can only pick up objects from limited directions, limiting the orientations in which the objects can be handled. Therefore, for future stages, it is essential to test and evaluate different types of end-effectors, such as suction or soft grippers. Potentially, we may need to design a unique gripper suitable for any meat processing operations.

Exchangeable tools

The project developed shadow robot system that can be used in different meat processing scenarios for different operations, in which the robotic arms need to attached with different tools, such as knives, hooks and dehiders. These tools can be attached with handles that are portable to quick changers on the arm’s end-effectors.

Communication and long-distance remote operations

Currently, the system is communicating through a host computer. Robotic arms, grippers, the host computer and the exoskeleton device, are connected to a local communication network and exchange data and commands locally. In order to achieve remote operations from different locations, we will need to connect all equipment to the Internet and establish a stable and secure communication network. We will need to investigate delays, cybersecurity issues and other constraints that can potentially affect the communication and performance of the system.

Real-time motoring and observation

While operating from a different location, the operator will need to rely on real-time image feeds to get feedback and control the operations. Cameras overviewing the working stations and attached to the robotic arms are required. We will need to estimate how to set up a monitoring system to allow the operators to have a sufficient and accurate view of the operations so that they can operate the robotic arms precisely.

Operator interface

The project is currently at the concept designing stage, and it still has a long way to go before production. An operator interface can be developed to display real-time data of the equipment, such as sensing human joint angles and robotic arm coordinates. The interface will also provide real-time camera images for the operator to observe the situations. The system will also record operational logs that can be used for further evaluations and improvements. It can also be implemented with AI support functions which will, potentially, predict human motions and evaluate the effectiveness of current operations. The interface can then guide human operations.

Operator training

With the wearable exoskeleton, the operators can easily operate the robotic arms by moving their arms, and the transfer matrix has converted the human poses into the robotic arm poses. However, the robot joint configurations and arm lengths are different from humans. It will take some time for the operators to get familiar with how to control the robotic arms precisely. However, for any further development of the project, we will focus on improving usability to minimise training requirements and allow the operators to get familiar with controlling the arms sooner.

Safety features

Currently, we are using the UR5 collaborative robotic arms as physical testing platforms, and the system relies on the hardware’s built-in safety features, such as the collision stops. If the emergency stops are triggered, the robotic arms will need to be manually reset to resume the control program. For future work, we can implement some soft safety

features, such as limiting their operation range and avoiding collision with pre-known equipment in the environment (e.g. the other arm and the arm base), which will reduce the number of incidences of triggering the emergency stops.

Production environment readiness

To ensure the functionality of the shadow robot in the meat processing facilities, we will implement the system with high tolerance, robust and reliable equipment that can be used in conditions with high-temperature steam, cold temperature and humidity. For example, UR5 robotic arms can be used with waterproofed covers yet still need to investigate for their reliability in a washdown high moisture processing environment. We may need to select different equipment that is feasible to be used in the meat processing environment. In addition, we will also need to design a framework for operational environment setup, which include all equipment and requirements before using the designed shadow robot, and, for any new installation in the future, the framework needs to be implemented and assessed.

7.0 Conclusions / Recommendations

Based on the project discovery and development, we found that the designed shadow robot has the potential to be used in multiple meat processing scenarios to replace humans in high-risk operations.

With the initial idea of the project, the operator can control shadow robot to portion products such as Osso Bucco through a bandsaw. However, we will need to reconfigure the setting and position the bandsaw station within the feasible operational zone, and the base of the robotic arms needs to rotate 90 degrees vertically to allow more flexible movements on the operating surface of the bandsaw. In addition, this process is a fast operation, and the safe speed limit of UR5 collaborative robotic arms needs to be removed or, alternatively, we can replace the robotic arms with other conventional robotic arms that have higher joint speed.

The shadow robot can also be used to debone meat parts. For example, we can hang the beef hindquarter on the overhead rails between the robotic arms. One side of the arm will be attached with a meat hook, and the other arm will be attached with a knife. The operator can control the robotic arms with the same motions as they are deboning manually. The hook side can hold and tear the removing parts, and the knife can cut through the tissue between muscles. Both end-effectors will need to be developed based on the required motions and functions.

The shadow robot can also be used to hold large electrical-powered tools such as carcass splitting bandsaws and head cutters. The shadow robot can be installed on the station where the human operators are standing, and no additional modifications are required in the processing facilities. The tools will be attached to the robotic arm, and the operators can control the shadow robot to perform the original tasks from a safe distance. While operating heavy tools, we may need to use robotic arms with higher payloads. Compared with conventional robotic equipment, the shadow robot does not require sensing and detection on the cutting paths, and human-controlled operations will be more flexible.

For the next stage, we can focus on,

- Design a feasible scenario that allows the shadow robot to be used in meat processing
- Improve the current exoskeleton device to enhance human motion detection
- Develop a remote-control framework to allow operators to control the shadow robot from different locations
- Develop operational safety standards to limit the robot motions within the effective operational zone and standardise human control operations

8.0 Bibliography

N/A

9.0 Appendices

9.1 Appendix 1

Human arm frames to robotic arm frame transformation functions:

$Frame_{Base}: B_0 \rightarrow B_2$				
i	α_{i-1}	a_{i-1}	d_i	θ_i
1	ω_1	0	0	0
2	0	0	0	$\frac{\pi}{2}$

$$ {}^{0}_{2}T_B = {}^{0}_{1}T_B\,{}^{1}_{2}T_B = \begin{bmatrix} 0 & -1 & 0 & 0 \\ cos(\omega_1) & 0 & -sin(\omega_1) & 0 \\ sin(\omega_1) & 0 & cos(\omega_1) & 0 \\ 0 & 0 & 0 & 1 \end{bmatrix} $$

$Frame_{ShoulderTwist}: St_0 \rightarrow St_4$				
i	α_{i-1}	a_{i-1}	d_i	θ_i
1	0	0	l_1	0
2	$\frac{\pi}{2}$	0	0	0
3	0	l_2	0	0
4	0	0	0	ω_2

$$ {}^{0}_{4}T_{St} = {}^{0}_{1}T_{St}\,{}^{1}_{2}T_{St}\,{}^{2}_{3}T_{St}\,{}^{3}_{4}T_{St} = \begin{bmatrix} cos(\omega_2) & -sin(\omega_2) & 0 & l_2 \\ 0 & 0 & -1 & 0 \\ sin(\omega_2) & cos(\omega_2) & 0 & l_1 \\ 0 & 0 & 0 & 1 \end{bmatrix} $$

$Frame_{ShoulderTension}: Sn_0 \rightarrow Sn_3$				
i	α_{i-1}	a_{i-1}	d_i	θ_i
1	0	l_3	0	0
2	0	0	0	$\frac{\pi}{2}$
3	$\frac{3\pi}{2}$	0	0	0

$$ {}^{0}_{3}T_{Sn} = {}^{0}_{1}T_{Sn}\,{}^{1}_{2}T_{Sn}\,{}^{2}_{3}T_{Sn} = \begin{bmatrix} 0 & 0 & -1 & l_3 \\ 1 & 0 & 0 & 0 \\ 0 & -1 & 0 & 0 \\ 0 & 0 & 0 & 1 \end{bmatrix} $$

$Frame_{ElbowTwist}: Et_0 \rightarrow Et_3$

i	α_{i-1}	a_{i-1}	d_i	θ_i
1	0	0	$-l_4$	0
2	0	0	0	$-\frac{\pi}{2}$
3	$\frac{\pi}{2}$	0	0	0

$$ {}^{0}_{3}T_{Et} = {}^{0}_{1}T_{Et}\,{}^{1}_{2}T_{Et}\,{}^{2}_{3}T_{Et} = \begin{bmatrix} 0 & 0 & -1 & 0 \\ -1 & 0 & 0 & 0 \\ 0 & 1 & 0 & -l_4 \\ 0 & 0 & 0 & 1 \end{bmatrix} $$

The transfer matrix from the base frame to the wrist frame is,

$$ \begin{bmatrix} \sigma_{11} & \sigma_{12} & \sigma_{13} & \sigma_{14} \\ \sigma_{21} & \sigma_{22} & \sigma_{23} & \sigma_{24} \\ \sigma_{31} & \sigma_{32} & \sigma_{33} & \sigma_{34} \\ 0 & 0 & 0 & 1 \end{bmatrix} $$

where,

$$ \sigma_{11} = \cos(\theta_{En})\left(\cos(\theta_{Et})\cos(\theta_{St}) + \sin(\theta_{Et})\sin(\theta_{St})\left(\frac{\sin(\theta_{Sn})}{2} + \frac{\sqrt{3}\cos(\theta_{Sn})}{2}\right)\right) + \sin(\theta_{En})\sin(\theta_{St})\left(\frac{\cos(\theta_{Sn})}{2} - \frac{\sqrt{3}\sin(\theta_{Sn})}{2}\right), $$

$$ \sigma_{12} = \cos(\theta_{En})\sin(\theta_{St})\left(\frac{\cos(\theta_{Sn})}{2} - \frac{\sqrt{3}\sin(\theta_{Sn})}{2}\right) - \sin(\theta_{En})\left(\cos(\theta_{Et})\cos(\theta_{St}) + \sin(\theta_{Et})\sin(\theta_{St})\left(\frac{\sin(\theta_{Sn})}{2} + \frac{\sqrt{3}\cos(\theta_{Sn})}{2}\right)\right), $$

$$ \sigma_{13} = \cos(\theta_{St})\sin(\theta_{Et}) - \cos(\theta_{Et})\sin(\theta_{St})\left(\frac{\sin(\theta_{Sn})}{2} + \frac{\sqrt{3}\cos(\theta_{Sn})}{2}\right), $$

$$ \sigma_{14} = -\frac{3298\sin(\theta_{St})}{25} - \frac{8713\sin(\theta_{St})\left(\frac{\cos(\theta_{Sn})}{2} - \frac{\sqrt{3}\sin(\theta_{Sn})}{2}\right)}{50}, $$

$$ \sigma_{21} = \sin(\theta_{En})\left(\frac{\sin(\theta_{Sn})}{4} + \frac{\sqrt{3}\cos(\theta_{Sn})}{4} - \frac{\sqrt{3}\cos(\theta_{St})\left(\frac{\cos(\theta_{Sn})}{2} - \frac{\sqrt{3}\sin(\theta_{Sn})}{2}\right)}{2}\right) - \cos(\theta_{En})\left(\sin(\theta_{Et})\left(\frac{\cos(\theta_{Sn})}{4} - \frac{\sqrt{3}\sin(\theta_{Sn})}{4} + \frac{\sqrt{3}\cos(\theta_{St})\left(\frac{\sin(\theta_{Sn})}{2} + \frac{\sqrt{3}\cos(\theta_{Sn})}{2}\right)}{2}\right) - \frac{\sqrt{3}\cos(\theta_{Et})\sin(\theta_{St})}{2}\right), $$

$$ \sigma_{22} = \cos(\theta_{En})\left(\frac{\sin(\theta_{Sn})}{4} + \frac{\sqrt{3}\cos(\theta_{Sn})}{4} - \frac{\sqrt{3}\cos(\theta_{St})\left(\frac{\cos(\theta_{Sn})}{2} - \frac{\sqrt{3}\sin(\theta_{Sn})}{2}\right)}{2}\right) + \sin(\theta_{En})\left(\sin(\theta_{Et})\left(\frac{\cos(\theta_{Sn})}{4} - \frac{\sqrt{3}\sin(\theta_{Sn})}{4} + \frac{\sqrt{3}\cos(\theta_{St})\left(\frac{\sin(\theta_{Sn})}{2} + \frac{\sqrt{3}\cos(\theta_{Sn})}{2}\right)}{2}\right) - \frac{\sqrt{3}\cos(\theta_{Et})\sin(\theta_{St})}{2}\right), $$

$$ \sigma_{23} = \cos(\theta_{Et})\left(\frac{\cos(\theta_{Sn})}{4} - \frac{\sqrt{3}\sin(\theta_{Sn})}{4} + \frac{\sqrt{3}\cos(\theta_{St})\left(\frac{\sin(\theta_{Sn})}{2} + \frac{\sqrt{3}\cos(\theta_{Sn})}{2}\right)}{2}\right) + \frac{\sqrt{3}\sin(\theta_{Et})\sin(\theta_{St})}{2}, $$

$$ \sigma_{24} = \frac{1649\sqrt{3}\cos(\theta_{St})}{25} - \frac{8713\sqrt{3}\cos(\theta_{Sn})}{200} - \frac{8713\sin(\theta_{Sn})}{200} + \frac{8713\sqrt{3}\cos(\theta_{St})\left(\frac{\cos(\theta_{Sn})}{2} - \frac{\sqrt{3}\sin(\theta_{Sn})}{2}\right)}{100} - \frac{2667}{100}, $$

$$ \sigma_{31} = -\sin(\theta_{En})\left(\frac{\cos(\theta_{St})\left(\frac{\cos(\theta_{Sn})}{2} - \frac{\sqrt{3}\sin(\theta_{Sn})}{2}\right)}{2} + \frac{\sqrt{3}\left(\frac{\sin(\theta_{Sn})}{2} + \frac{\sqrt{3}\cos(\theta_{Sn})}{2}\right)}{2}\right) - \cos(\theta_{En})\left(\sin(\theta_{Et})\left(\frac{\cos(\theta_{St})\left(\frac{\sin(\theta_{Sn})}{2} + \frac{\sqrt{3}\cos(\theta_{Sn})}{2}\right)}{2} - \frac{\sqrt{3}\left(\frac{\cos(\theta_{Sn})}{2} - \frac{\sqrt{3}\sin(\theta_{Sn})}{2}\right)}{2}\right) - \frac{\cos(\theta_{Et})\sin(\theta_{St})}{2}\right), $$

$$ \sigma_{32} = \sin(\theta_{En})\left(\sin(\theta_{Et})\left(\frac{\cos(\theta_{St})\left(\frac{\sin(\theta_{Sn})}{2} + \frac{\sqrt{3}\cos(\theta_{Sn})}{2}\right)}{2} - \frac{\sqrt{3}\left(\frac{\cos(\theta_{Sn})}{2} - \frac{\sqrt{3}\sin(\theta_{Sn})}{2}\right)}{2}\right) - \frac{\cos(\theta_{Et})\sin(\theta_{St})}{2}\right) - \cos(\theta_{En})\left(\frac{\cos(\theta_{St})\left(\frac{\cos(\theta_{Sn})}{2} - \frac{\sqrt{3}\sin(\theta_{Sn})}{2}\right)}{2} + \frac{\sqrt{3}\left(\frac{\sin(\theta_{Sn})}{2} + \frac{\sqrt{3}\cos(\theta_{Sn})}{2}\right)}{2}\right), $$

$$\sigma_{33} = \cos(\theta_{Et})\left(\frac{\cos(\theta_{St})\left(\frac{\sin(\theta_{Sn})}{2}+\frac{\sqrt{3}\cos(\theta_{Sn})}{2}\right)}{2} - \frac{\sqrt{3}\left(\frac{\cos(\theta_{Sn})}{2}-\frac{\sqrt{3}\sin(\theta_{Sn})}{2}\right)}{2}\right) + \frac{\sin(\theta_{Et})\sin(\theta_{St})}{2}, \text{ and}$$

$$\sigma_{34} = \frac{1649\cos(\theta_{St})}{25} + \frac{2667\sqrt{3}}{100} + \frac{8713\cos(\theta_{St})\left(\frac{\cos(\theta_{Sn})}{2}-\frac{\sqrt{3}\sin(\theta_{Sn})}{2}\right)}{100} + \frac{8713\sqrt{3}\left(\frac{\sin(\theta_{Sn})}{2}+\frac{\sqrt{3}\cos(\theta_{Sn})}{2}\right)}{100}.$$

Therefore, the wrist coordinates are,

$$x = -\frac{3298\sin(\theta_{St})}{25} - \frac{8713\sin(\theta_{St})\left(\frac{\cos(\theta_{Sn})}{2}-\frac{\sqrt{3}\sin(\theta_{Sn})}{2}\right)}{50},$$

$$y = \frac{1649\sqrt{3}\cos(\theta_{St})}{25} - \frac{8713\sqrt{3}\cos(\theta_{Sn})}{200} - \frac{8713\sin(\theta_{Sn})}{200} + \frac{8713\sqrt{3}\cos(\theta_{St})\left(\frac{\cos(\theta_{Sn})}{2}-\frac{\sqrt{3}\sin(\theta_{Sn})}{2}\right)}{100} - \frac{2667}{100}, \text{ and}$$

$$z = \frac{1649\cos(\theta_{St})}{25} + \frac{2667\sqrt{3}}{100} + \frac{8713\cos(\theta_{St})\left(\frac{\cos(\theta_{Sn})}{2}-\frac{\sqrt{3}\sin(\theta_{Sn})}{2}\right)}{100} + \frac{8713\sqrt{3}\left(\frac{\sin(\theta_{Sn})}{2}+\frac{\sqrt{3}\cos(\theta_{Sn})}{2}\right)}{100}.$$

9.2 Appendix 2

Link to the BOX folder with testing videos:

https://universityofadelaide.box.com/s/65p5lfdr795rjkgix16680zhlnsxkv5e

Password: AMPCUoA2022

9.3 Appendix 3

Key specifications of physical equipment:

8.3.1 UR5e robotic arms

The project is designed to have two robotic arms controlled by a human operator. UoA has purchased UR5e robotic arms, and each of these arms has the following key specifications,

Payload	5 kg	
Reach	850 mm	
Degrees of freedom	6 rotating joints	
Power, consumption, maximum average	570 W	
Power, consumption, typical, with moderate settings	200 W	
Power source	100-240VAC, 47-440Hz	
Axis movement	Working range	Maximum speed
Base	± 360°	± 180°/s
Shoulder	± 360°	± 180°/s
Elbow	± 360°	± 180°/s
Wrist 1	± 360°	± 180°/s
Wrist 2	± 360°	± 180°/s
Wrist 3	± 360°	± 180°/s
Footprint	Ø 149 mm	
Total weight	20.6 kg (arm) + 12 kg (control box) + 1.6 (teach pendant)	
I/O Power supply	24V 2A	
Control frequency	500 Hz	

8.3.2 OnRobot RG6 gripper

The project is designed to use the OnRobot RG6 grippers to grab and hold the processing parts. The fingertip may need to be redesigned and exchanged while processing different parts. The key specifications of the RG6 grippers are listed in the following table.

Payload force (vertical)	6 kg
Payload force (horizontal)	10 kg

Total stroke (adjustable)	160 mm
Finger position resolution	0.1 mm
Gripping force	25 – 120 N
Gripping speed	51 – 160 mm/s
Power supply	24 V
Current consumption	70 – 600 mA
Calculated operation life	30,000 hours